ACS APPLIED MATERIALS & INTERFACES

Research Article

www.acsami.org

Nitrogen-Doped Mesoporous Graphene as a Synergistic Electrocatalyst Matrix for High-Performance Oxygen Reduction Reaction

Jingjing Xiao,[†] Xiaojun Bian,[†] Lei Liao,[†] Song Zhang,[†] Chang Ji,[‡] and Baohong Liu*[,†]

[†]Department of Chemistry, State Key Lab of Molecular Engineering of Polymers and Collaborative Innovation Center of Chemistry for Energy Materials, Fudan University, Shanghai 200433, China

[‡]Department of Chemistry and Biochemistry, Texas State University, 601 University Drive, San Marcos, Texas 78666, United States

Supporting Information

ABSTRACT: To balance the anchoring sites and conductivity of the catalyst supports is a dilemma in electrocatalytic oxygen reduction reaction (ORR). Nitrogen-doped mesoporous graphene (N-MG) with large surface area, high porosity, and superior intrinsic conductivity has been developed to address this issue. Using N-MG as the backbone, a hybrid catalyst of Co_3O_4 nanocrystals embedded on N-MG (Co_3O_4/N-MG) was prepared for the electrocatalytic ORR in alkaline media. The Co_3O_4/N-MG showed high catalytic activity for the four-electron ORR, giving a more positive onset potential (0.93 V vs RHE) and a higher current density. The unique property of N-MG and the synergetic effect of Co_3O_4 and N-MG are prominent for ORR. With improved electrocatalytic activity and durability, the Co_3O_4/N-MG can be an efficient nonprecious metal catalyst and potentially used to substitute the platinum-based cathode catalysts in fuel cells and metal−air batteries.

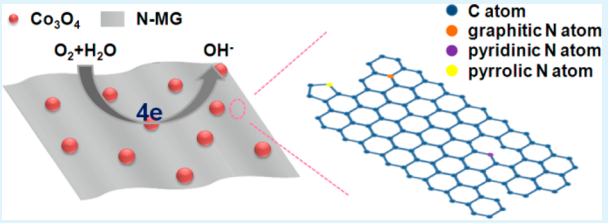

KEYWORDS: *nitrogen-doped mesoporous graphene, catalyst, cobalt oxide, oxygen reduction reaction, electrocatalysis*

INTRODUCTION

In recent years, it has become more urgent and inspiring to find clean and cheap energy to meet the rapid increase in global demand. Without the limit of energy-conversion efficiency caused by Carnot cycle, and due to the advantages of low emission, high energy density, reusability, and environmental benignity, fuel cells (FCs) as well as metal−air batteries have been intensively studied as the promising energy sources for the future.[1−3] The major obstacle for the extensive application of these technologies is caused by the sluggish oxygen reduction reaction (ORR) at the cathode side.[4] Platinum (Pt) is the most commonly used ORR catalyst because it requires the lowest overpotential to generate a certain current.[5] Nevertheless, Pt may not perform well as expected in many occasions, attributed to the degradation of its catalytic activity and the lack of methanol tolerance. Moreover, the low abundance of Pt on earth causes the exceptionally high price for its consumption. Consequently, much attention has been drawn to develop nonprecious metal (NPM) based electrocatalysts to replace the Pt catalysts.[6,7]

Cobalt-based catalysts such as cobalt sulfides, cobalt corroles, and other cobalt compounds have received widespread interests ever since Jasinski first discovered the catalytic property of cobalt phthalocyanine for ORR in 1964.[8−10] Among these materials, cobaltosic oxide (Co_3O_4) is particularly attractive because of its typical spinel crystalline structure, which has been well-known as the electrocatalytic active form for NPM based catalysts.[11] Though great efforts have been made to develop various cobalt catalysts for ORR, their general performance is still less than satisfactory.[12] To adopt a different strategy by using some novel catalyst supports for improvement is therefore of paramount importance.

Due to their unique electrical and mechanical properties, carbon materials have been employed as efficient catalyst supports in FCs to reduce the loading of catalysts while still render better catalytic activity, durability, and conductivity.[12] Reduced graphene oxide, carbon nanotubes, and mesoporous carbons have all been used as supports for cobalt oxides to catalyze ORR with better performance.[11,13−15] Graphene, a single-atom-thick carbon nanosheet, possesses large specific area, strong mechanical strength, as well as high electroconductivity and corrosion-resistance. These properties make it a promising material as catalyst support.[11] However, the lack of highly reactive edge sites in graphene and the tendency of stacking together are detrimental to the catalysts coating and reactants diffusion.[16] Functional groups on graphene (which is properly oxidized) could be beneficial for the nucleation and anchoring of nanocrystals on the sheets to achieve covalent attachments but may otherwise lower the electroconductivity

Received: June 18, 2014
Accepted: September 29, 2014
Published: September 29, 2014

and put a limit on the catalytic efficiency of the hybrid materials.[13,17]

To address these aforementioned issues, we developed an advanced material of nitrogen doped mesoporous graphene (N-MG) as the NPM catalyst support. With its hydrophobic nature, the mesoporous graphene is expected to easily accommodate the metal oxide nanoparticles.[18] The doped nitrogen atoms would also act as anchoring sites and strengthen the bonding between the catalyst and the carbon surface to help dispersion of the catalyst particles so that the activity and durability of the hybrid catalyst will be enhanced.[12] Besides, the increase of nitrogen content in carbon can also help to create a metal-like conductivity,[19] which would favor a better electrical communication among the electrode, catalyst, and reactants to make full use of the active sites in the material. Moreover, the change of charge density for the atoms in graphitic framework due to the presence of nitrogen could provide a desirable electronic structure to improve the adsorption and reduction of molecular oxygen.[12,20] Furthermore, the three-dimensional (3D) structure of N-MG not only can prevent graphene sheets from stacking but also can facilitate the diffusion of reactants and allow rapid charge transfer during electrocatalysis. All these factors make N-MG a preferable electrocatalyst support for ORR.

In this study, N-MG was successfully used as the substrate to load Co_3O_4 nanocrystals. The resulting Co_3O_4/N-MG hybrid catalyst outperformed the mesoporous graphene (MG), the nitrogen-doped graphene (N-G) counterparts, and Pt/C (10 wt % platinum on Vulcan carbon) in terms of both half-wave potential and current density for ORR in 0.1 M KOH, showing that N-MG is an excellent support as more catalytically active sites are formed in the hybrid. Various materials were also employed to examine the matrix impact as well as the interactions between the catalyst and the support. Different ratios and methods of doping nitrogen atoms were used for optimizing the performance of Co_3O_4/N-MG nanocomposites.

MATERIALS AND METHODS

Reagents. Pluronic F108, dimethoxydimethylsilane (DMDMS, 95%), cobalt(II) acetate ($Co(Ac)_2$, 99.995%), Pt/C (10 wt % platinum on Vulcan carbon), and Nafion perfluorinated ion-exchange resin solution (5% w/w) were purchased from Sigma-Aldrich. Tetraethyl orthosilicate (TEOS), 1,3,5-trimethylbenzene (TMB), and melamine (99%) were obtained from Shanghai Chemical Plant. Graphite oxide (GO, 99%) was bought from Nanjing XianFeng Nano Material Technology Co. Ltd. Deionized water was used to prepare aqueous solutions. All chemicals were used as received without further treatment.

Synthesis of N-MG. N-MG was synthesized by using hollow siliceous spheres (HSSs) as the hard template and GO as the carbon source. Melamine was selected as the nitrogen precursor since it can be removed completely at high temperature.[18,20] HSSs were prepared according to the literature procedures.[21] Typically, 1.0 g of Pluronic F108 and 1.0 g of TMB were dissolved into 2 M of aqueous HCl solution (30 mL) and stirred for 12 h at room temperature (RT). Subsequently, 1.0 g of TEOS was added dropwise and after stirring for another 6 h at RT, 0.5 g of DMDMS was introduced, and the reaction was set to run for 48 h. The resulting suspension was dialyzed in deionized water for 48 h to remove HCl. After that, 30 mL of deionized water was added into the dialyzed suspension, and the mixture was sonicated for half an hour to obtain the diluted HSSs/H_2O solution. Meanwhile, 0.6 g of GO was dispersed into 600 mL of deionized water. The suspension was mixed with the HSSs solution mentioned above and stirred for 24 h to produce the self-assembled GO/HSSs composite. Because of the hydrophobic interaction between the methyl group functionalized SiO_2 nanospheres and GO sheets, GO can self-assemble on the outside of SiO_2. The precipitates were collected by centrifugation at 4500 rpm and dried at 50 °C. Finally, the dried material (ca. 2.0 g) was ground with 4.0 g of melamine. The fine powder mixture was heated to 900 °C with a ramping rate of 5 °C min^{-1} and kept at 900 °C for 5 h. The calcination process was carried out under argon atmosphere. After removal of silica by HF (5 wt %) etching, the sample was washed by deionized water and dried in oven afterward. In this way, the 3D structure was maintained and pores were formed after removing silica templates. For comparison purposes, pure MG was synthesized by the similar steps without adding melamine in the process.

Synthesis of Co_3O_4/N-MG. Co_3O_4/N-MG was prepared by a modified literature method.[14] Generally, 18.8 mg of N-MG and 20 mL of anhydrous ethanol (EtOH) were mixed and sonicated for 30 min to achieve good dispersion. Followed by the addition of 4.0 mL of well dispersed $Co(Ac)_2$/EtOH suspension (4.6 mg mL^{-1}), the solution was sonicated for another 10 min. Afterward, 2.4 mL of deionized water was introduced and the mixture was stirred at 80 °C using an oil bath for 12 h. The reaction mixture was then transferred to autoclave and kept at 150 °C for 3 h for hydrothermal reaction, which led to the growth of Co_3O_4 nanocrystals on N-MG sheets. After centrifugation, the product was collected and washed by EtOH and deionized water successively and dried in vacuum to obtain the final catalyst hybrid. Hybrids with different Co_3O_4 mass loading were prepared by changing the ratio of $Co(Ac)_2$ to N-MG.

For the syntheses of Co_3O_4/N-G, Co_3O_4/MG, and Co_3O_4, the same method was used as discussed above by simply replacing N-MG with N-G or MG or without the carbon support in the first step. Co_3O_4/MG-N was obtained by adding 1.8 mL of deionized water and 0.6 mL of NH_4OH (28 wt %) (rather than pure deionized water) to the mixture of MG and $Co(Ac)_2$ suspension for the hydrothermal reaction by similar steps.

Characterization. Atomic force microscopy (AFM) measurements were carried out by a Bruker Dimension Icon in tapping mode. Transmission electron microscopy (TEM) images were recorded by a JEOL JEM-2011 electron microscope with an acceleration voltage of 200 kV. Scanning electron microscopy (SEM, Nova NanoSEM207) equipped with energy dispersive spectroscopy (EDS) was used to characterize the materials. The specific surface area and pore size distribution were derived from the nitrogen adsorption/desorption isotherm (acquired by Quantachrome's Quadrasorb SI analyzer) by using BET and BJH methods, respectively. X-ray photoelectron spectroscopy (XPS) data were collected by an X-ray photoelectron spectrometer (PerkinElmer PHI 5000C ESCA System) equipped with Mg Kα radiation. X' Pert PRO (PANalytical, Cu Kα radiation) was used to get the X-ray diffraction (XRD) patterns. Raman spectra were taken by a Labram-1B Raman spectrometer from Yobin Yvon with a laser (2 mW) excitation wavelength of 632.8 nm.

Electrode Preparation and Electrochemical Analysis. First, 2.5 mg of Co_3O_4/N-MG (or other catalysts) was dispersed into a mixture composed of 5 wt % Nafion solution (8 μL) and 3:1 v/v water/isopropanol (0.5 mL) by 1 h of sonication to form a homogeneous ink. Subsequently, a certain amount (33 μg) of the catalyst ink was dropped on the polished glassy carbon rotating disk electrode (GC RDE, 5 mm in diameter) to give a catalyst loading of about 170 μg cm^{-2}. The electrochemical studies were conducted in a conventional three-electrode cell by using RDE (MSR Electrode Rotator by CE Mark) as the working electrode. The saturated calomel electrode (SCE) was used as a reference and a Pt foil served as the counter electrode. All the potentials reported herein were calibrated with respect to the reversible hydrogen electrode (RHE) according to the Nernst equation. CHI 660C electrochemical workstation and CTV101 speed control unit were also employed for the electrochemical analyses and the RDE experiments. All ORRs were examined in 0.1 M KOH saturated with O_2 (or N_2 for comparison) at RT. Electrochemical impedance spectroscopy (EIS) was carried out in 10 mM of $Fe(CN)_6^{-3/-4}$ solution at open circuit potential by AutoLab PGSTST 30 analyzer (Metrohm Autolab B.V., Switzerland) over a frequency range from 10^5 to 10^{-1} Hz with a single modulated AC

potential of 10 mV. EIS data were analyzed and fitted by using NOVA 1.7.

RESULTS AND DISCUSSION

Characterization of N-MG and Co_3O_4/N-MG. N-MG was prepared from graphene oxide (GO) by a thermal annealing approach using HSSs as the template and melamine as the nitrogen source. AFM was employed to characterize the morphology of N-MG. The thickness of N-MG sheet is around 0.55 nm (as shown by Figure 1a), indicating that the material

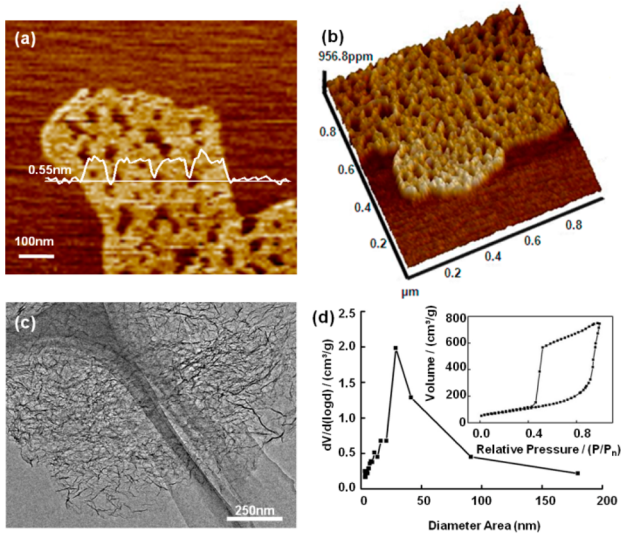

Figure 1. 2D (a) and 3D (b) AFM view of N-MG obtained with NanoScope Analysis v1.40 software. (c) TEM image of N-MG. (d) N_2 adsorption/desorption isotherms (inset) and the corresponding pore size distribution of N-MG.

contains only 1 to 2 atomic carbon layers (theoretically, the thickness of a single-layer graphene is 0.34 nm). The 3D view (Figure 1b) displays the porosity of N-MG, which is also observed by TEM (Figure 1c) and SEM images (Supporting Information Figure S1). The successful preparation of N-MG with limited number of layers can be credited to the self-assembly taking place between GO sheets and the hydrophobic templates of HSSs, rather than the aggregation and stacking of GO sheets themselves. The porous property of N-MG was further investigated by N_2 adsorption/desorption isotherms. The type IV isotherm with hysteresis characteristic presented in Figure 1d (inset) indicates the existence of mesopores in N-MG.[22] The pore size mainly ranges from 20 to 40 nm (Figure 1d), which would be favorable for the easy access to reactants and the formation of gas-electrode−electrolyte triple-phase boundary that consequently enhances the electrochemical activity of NPM catalysts. The high surface area (1599 m^2 g^{-1}) of N-MG, caused by its porous structure, could also contribute to a better dispersion of catalyst nanoparticles with more active sites available for reactants. All these properties are important for surface reactions like ORR.[11]

The elemental composition and properties of N-MG were probed by XPS. All the binding energies in XPS spectra were calibrated by using the carbonaceous C 1s line (284.6 eV) as the reference. Figure 2a reveals the distinct C 1s, N 1s, and O 1s signals of N-MG and the corresponding content of nitrogen is estimated to be 2.8 at%. The N 1s spectrum was deconvoluted to study the bonding configurations of nitrogen

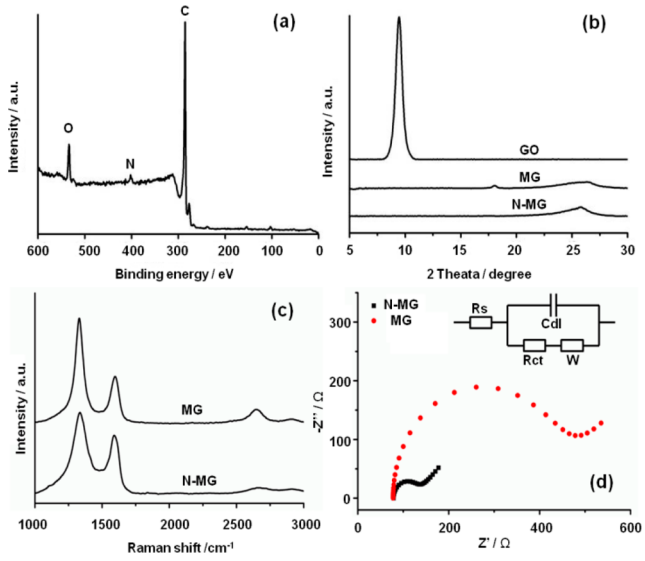

Figure 2. (a) Full XPS spectrum of N-MG. (b) Typical XRD patterns of GO, MG, and N-MG (from top to bottom). (c) Raman spectra of MG and N-MG. (d) Nyquist plots of N-MG and MG modeled by equivalent electrical circuit (inset).

atoms in N-MG. As illustrated in Supporting Information Figure S2a, four individual peaks are correlated to different types of nitrogen, namely, pyridinic nitrogen (398.4 eV), pyrrolic nitrogen (400.5 eV), graphitic nitrogen (401.4 eV), and oxidized nitrogen (403.6 eV).[23] The pyridinic and pyrrolic nitrogen refer to sp^2-hybridized nitrogen atoms that can donate one or two p-electrons to the π-conjugated system, while the graphitic nitrogen atoms are those doped into the graphene layers by substituting the carbon atoms in hexagonal rings.[7,24,25] The bonding configurations of carbon atoms were also examined (Supporting Information Figure S2b). Likewise, the main peak around 284.5 eV suggests that most carbon atoms should be the sp^2-hybridized graphitic carbon. The other smaller peak at 285.8 eV demonstrates the existence of C−N bonds. All these results confirm the successful nitrogen doping and reduction of graphene oxides in the material. Some oxygen-containing groups (288.0 eV) are still retained after thermal annealing, which can facilitate the nucleating of catalysts on N-MG.[13,16]

XRD patterns of N-MG and GO are compared in Figure 2b. The vanishing of the characterized GO peak and the formation of graphene crystallographic plane (002) at 26.6° (2θ)[26] further verify the graphitic framework in N-MG. Mesoporous graphene (MG) was also made for control experiment. The XRD peak of (002) plane for MG is broader than that of N-MG, indicating there are smaller size of graphene layers and lower degree of crystallinity in MG. Additionally, the *d*-spacing of MG (3.36 Å) is little bigger than that of N-MG (3.35 Å, which is in accordance with the value for single-crystal graphite), likely due to a less efficient removal of oxygen in the MG sheets caused by the incomplete reduction of GO.[27] It has been reported that by the same annealing process, the oxygen content is lower in N-doped graphene than that in pristine graphene.[25] The EDS analysis also confirmed that N-MG contained fewer oxygen species than MG (ca. 9 and 13 wt %, respectively). Raman spectroscopy was carried out to extend the study for the carbon structures and qualities in N-MG (Figure 2c). The G band around 1590 cm^{-1} can be ascribed to the E_{2g} vibration of sp^2-hybridized carbon, which usually reflects the degree of

graphitization. On the other hand, the D band at 1336 cm^{-1} is related to disorders and defects in the structure. Similar peaks with different intensity ratio can be observed in the Raman spectrum of MG. The I_D/I_G value decreases from 2.25 for MG to 1.40 for N-MG, revealing that more GO have been restored to graphitic structure with the presence of nitrogen atoms,[20] as consistent with the XRD results. In comparison with MG, N-MG has higher reduction degree of GO to give a better conductivity, which is crucial for fast charge transfer during the oxygen reduction process to lower the electrical resistance and ensure the full utilization of the active catalytic sites.[11−13,25]

To compare the conductivity of both materials, EIS was applied to study MG and N-MG modified electrodes. The data were fitted by the equivalent circuit model and the corresponding Nyquist plots were depicted in Figure 2d. The results showed that N-MG modified electrode had a lower charge transfer resistance (R_{ct}) value of 51 Ω than that for MG modified electrode (357 Ω), indicating that N-MG exhibited higher electrical conductivity for the electron transfer between $Fe(CN)_6^{3-/4-}$ and the electrode. Most likely, the higher degree of graphitization in N-MG is related to the better conductivity. On the other hand, N-MG modified electrode also had a higher electrode−electrolyte interface capacitance (C_{dl}) value of 279.6 μF cm^{-2} while the capacitance of MG was 115.4 μF cm^{-2}, suggesting that the N-doped mesoporous graphene had a larger effective surface area.

Co_3O_4/N-MG hybrid nanocomposite (30 wt % Co_3O_4) was subsequently synthesized as the catalyst for ORR by using N-MG as the support. TEM image in Figure 3a clearly depicts the

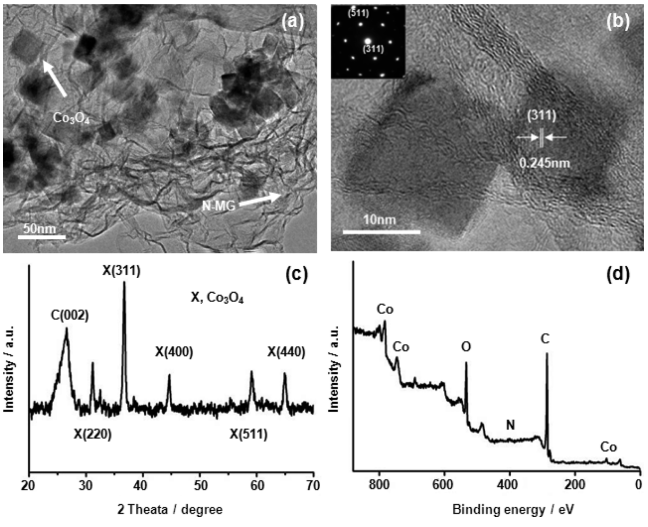

Figure 3. (a) TEM and (b) high magnification TEM images of Co_3O_4/N-MG with SAED pattern (inset). (c) Powder XRD spectrum and (d) XPS sweep scan of Co_3O_4/N-MG.

dispersed Co_3O_4 nanocrystals on N-MG and the size mainly ranges from 20 to 30 nm. The high resolution TEM image (Figure 3b) shows the *d* spacing of nanosized Co_3O_4. The selected area electron diffraction (SAED) pattern (Figure 3b inset) is in accordance with XRD analysis (Figure 3c), indicating the high crystallinity of Co_3O_4 nanoparticles. Characteristic XRD peaks for (220), (311), (400), (511), and (440) planes further confirm the cubic spinel structure of Co_3O_4 [JCPDS, No. 01-080-1534].[14] The *d* spacing data calculated for (311) planes (Figure 3b), for example, also agrees well with the theoretical value (0.245 nm). Additionally, the composition of Co_3O_4/N-MG is revealed by XPS (Figure 3d), showing the presence of all elements in the material.

Electrocatalytic Properties of Co_3O_4/N-MG Modified Electrodes for ORR. The electrocatalytic activity of Co_3O_4/N-MG for ORR was first studied by cyclic voltammetry (CV). Figure 4 displays the cyclic voltammograms (CVs) of Co_3O_4/

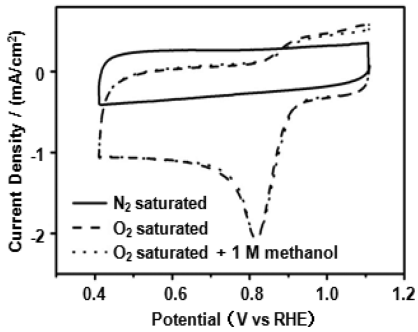

Figure 4. CVs for Co_3O_4/N-MG modified GC RDE in 0.1 M KOH solution saturated with N_2 (solid line), O_2 (dashed lines), and O_2 with 1 M CH_3OH (dotted lines) at a scan rate of 50 mV s^{-1}.

N-MG modified GC RDE in 0.1 M KOH under various conditions. When the KOH solution was saturated with nitrogen, no specific CV features could be observed in the scan window, while in the presence of oxygen, a well-defined cathodic peak showed up at 0.82 V with an onset potential around 0.93 V, demonstrating the catalytic activity of Co_3O_4/N-MG for ORR. Noticeably, there was no significant change in the CV for ORR after introducing methanol into the solution, indicating a high methanol tolerance of the hybrid Co_3O_4/N-MG nanomaterial, which could outperform the commercial Pt/C catalyst. For comparison, CVs of ORR using Pt/C as the catalyst are given in Supporting Information Figure S3, showing a similar onset potential as well as the strong interference by methanol.

Measurements for rotating disk electrode (RDE) modified with the catalyst were then carried out by linear sweep voltammetry (LSV) in O_2-saturated 0.1 M KOH. Polarization curves at different rotating speeds were recorded from 1.0 to 0.2 V with a scan rate of 5 mV s^{-1} to study the kinetics of the catalyzed ORR (Figure 5a). Typically, the current densities increase with the rotating speeds (from 400 to 2025 rpm). Sharp increase of the current density in the mixed kinetic-diffusion control region exhibits an efficient diffusion of the reactants, facilitated by the porous structure of the N-MG support. The subsequent current plateau points to the appearance of a diffusion-limiting region.[6] To better explain the ORR catalyzed by Co_3O_4/N-MG modified electrodes, the LSV data were analyzed using the Koutecky−Levich (K-L) equation (eq 1):

$$\frac{1}{j} = \frac{1}{j_k} + \frac{1}{j_l} = \frac{1}{j_k} + \frac{1}{0.62nFD_{O_2}^{2/3}\nu^{-1/6}C_{O_2}\omega^{1/2}} \quad (1)$$

where *j* is the measured current density; j_k and j_l are the kinetic and diffusion-limited current densities at a constant potential, respectively; *n* is the number of electrons transferred per O_2 molecule; *F* is the Faraday constant (96 485 C mol^{-1}); D_{O_2} is the diffusion coefficient of oxygen (1.9×10^{-5} cm^2 s^{-1}); *ν* is the kinematic viscosity of the solution (0.01 cm^2 s^{-1}); C_{O_2} is the bulk concentration of oxygen (1.2×10^{-6} mol cm^{-3}); and *ω* is

dx.doi.org/10.1021/am503895w | ACS Appl. Mater. Interfaces 2014, 6, 17654−17660

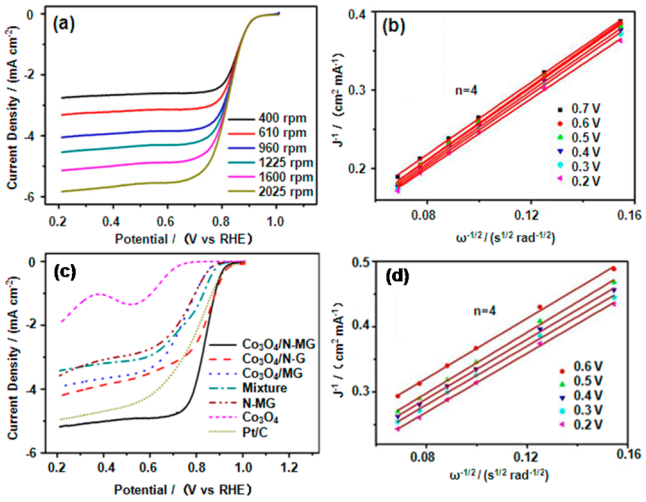

Figure 5. (a) LSVs for Co_3O_4/N-MG GC RDE recorded in O_2-saturated 0.1 M KOH solution at various rotating speeds with a scan rate of 5 mV s^{-1}. (b) The corresponding K-L plots from (a) at different potentials. (c) Comparative polarization curves for different catalysts with the same mass loading measured at 1600 rpm in O_2-saturated 0.1 M KOH. (d) K-L plots for Co_3O_4/MG calculated from Supporting Information Figure S4b.

the electrode rotating speed expressed in rps.[28,29] The K-L plots (j^{-1} vs $\omega^{-1/2}$) were created at various potentials, as presented in Figure 5b. The excellent linearity of the data indicates that the ORR rate obeys first-order kinetics with respect to the bulk oxygen concentration, while the nonzero intercepts of the extrapolated K-L regression lines confirm the mixed kinetic-diffusion controlled ORR process in a wide range of potentials.[30] The slopes of the linearly fitted K-L plots remain approximately the same at different potentials, and the *n* number derived from them on the basis of eq 1 is close to 4. The results suggest that oxygen should be reduced via a four-electron pathway at Co_3O_4/N-MG modified GC RDE, illustrating an efficient electrochemical ORR process.

Synergetic Effect for Enhanced ORR Catalytic Activity. The catalytic performance of Co_3O_4/N-MG hybrid catalyst was further compared with the other materials (Figure 5c). Co_3O_4/N-MG shows the best catalytic activity in terms of both half-wave potential and current density. Well-defined polarization curve indicates the rapid electron and mass transfer for ORR on Co_3O_4/N-MG modified electrode. In comparison, Co_3O_4/N-G has a similar half-wave potential, revealing the important influence of nitrogen incorporation on improving the catalytic efficiency of the hybrid material. Faster charge transfer and better utilization of catalytic active sites can be achieved due to the high conductivity of the hybrid with the presence of doped N atoms.[11,12,19] The change of charge density of the matrix, which could improve the adsorption and reduction of oxygen, also contributes to the better catalytic performance for ORR.[20] However, the lack of porosity in Co_3O_4/N-G causes a lower current density as the consequence. The porous structure can not only provide a high specific surface area but also facilitate the diffusion of reactants in the ORR process, which are key factors for higher current density. Without nitrogen doping, the hybrid catalyst (Co_3O_4/MG) gives a negative shift in half-wave potential and a deteriorated current density. These results show that Co_3O_4/N-MG, as the promising nanocomposite, possesses more efficient active sites for enhanced catalytic ORR. Noticeable positive shifts in the half-wave potential can also be observed for Co_3O_4/N-MG when compared with the other three materials (Co_3O_4, N-MG, and their mixture in Figure 5c), demonstrating the noteworthy synergistic effect of Co_3O_4 and N-MG (which exists exclusively in the case of the hybrid material) for higher catalytic activity in ORR. Moreover, the *n* numbers of ORR at N-MG and Co_3O_4 are not four (instead they are 2.9 and 3.1, respectively, Supporting Information Figure S4a), which would adversely affect both the energy efficiency and the life cycle of the catalysts since the formation of peroxide species may accelerate degradation of the materials.[7] As illustrated, the favorable changes of catalytic active sites in the hybrid through the interaction between the support and the catalyst turn the ORR into a more efficient reaction process.

With regard to the previous report that the reduction of oxygen might take place at the interface of Co_3O_4 nanocrystals and the catalyst support,[14] we changed the loading ratios of Co_3O_4 on N-MG to study this effect. As observed in Supporting Information Figure S5, a lower loading amount of Co_3O_4 in the hybrid catalyst (10 wt % loading ratio, Supporting Information Figure S5a) did not change the size of Co_3O_4 nanoparticles (ca. 25 nm) when compared to the loading ratio of 30 wt % (Figure 3a), but the corresponding catalytic activity for ORR obviously decreased (Supporting Information Figure S5c) as the number of active sites was reduced. The higher loading of Co_3O_4 was also unfavorable owing to the aggregation or free growth of the catalyst nanoparticles (Supporting Information Figure S5b), which could diminish the reaction surface area and impede the reactants from contacting the active sites.[13,31] It has also been proposed that nitrogen species may strengthen the bonding between the catalyst and the carbon surface, which would give a more powerful coupling effect between Co_3O_4 and N-MG to provide more efficient active sites.[12,24] This may rationalize the fact that Co_3O_4/MG hybrid also showed notable enhancement of catalytic performance (Figure 5c) with a similar electron transfer number of four (Figure 5d). Nevertheless, the corresponding current density was much lower when compared with Co_3O_4/N-MG (Figure 5c). EIS results have confirmed that N-MG possessed higher electroactive surface area, leading to the higher current density in catalytic ORR. On the other hand, the doped nitrogen could also change the surface chemistry of MG to affect the interaction between the support and the catalyst, which in turn modifies the electronic structure of the catalyst material and improves the performance of the resultant hybrid.[12] Changes of Co−O bonding in the hybrid, which is highly correlated to the catalytic activity for ORR, can take place as well due to the similar microenvironment alteration.[6,14] The microstructural changes for MG and N-MG in the hybrid catalysts can be observed in the comparison of Raman spectra (Supporting Information Figure S6a and Figure 2c), further proving that the Co_3O_4 nanoparticles have a mutual impact with the supporting materials. The improvement in carbon-catalyst bonding in Co_3O_4/N-MG can also be attested by its exceptional durability. There is little decay for the Co_3O_4/N-MG catalyzed ORR current (Figure 6) after 25 000 s of continuous polarization at 0.6 V. In contrast, more than 35% decrease in the corresponding reduction currents can be observed for both Co_3O_4/MG and Pt/C. As pointed out previously, the strong interaction between N-MG and Co_3O_4 would effectively increase the stability of catalyst nanoparticles and prevent them from agglomeration.[12] Moreover, although the carbon support is well-known for its good chemical stability,

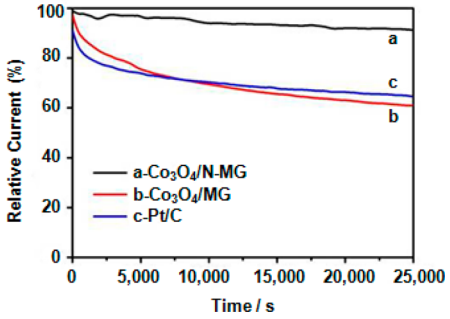

Figure 6. Chronoamperometric curves of (a) Co_3O_4/N-MG, (b) Co_3O_4/MG, and (c) Pt/C electrodes at 0.6 V in O_2-saturated 0.1 M KOH.

it can be slowly oxidized to carbon dioxide during extended operation at the cathode in fuel cells. Consequently, the performance of the hybrids would deteriorate as the corrosion of carbon support could cause the loss, agglomeration, and coalescence of the catalyst materials.[12] With the incorporation of nitrogen into MG structure, the support could be much less prone to oxidation, contributing to the good stability of Co_3O_4/N-MG.[19,32,33]

The crystallization of Co_3O_4 on N-MG also differs from that on MG. As revealed by the TEM images, the organized distribution of Co_3O_4 nanocrystals on N-MG is better than that on MG (Figure 3b and Supporting Information Figure S6b, respectively). Well-defined dots (Figure 3b inset) rather than rings (Supporting Information Figure S6b inset) are also observed in the diffraction pattern of Co_3O_4/N-MG, suggesting a more ordered texture of the Co_3O_4 nanocrystals. This result may be attributed to the stronger binding energy of C with Co_3O_4 where carbon atoms are close to nitrogen atoms, which would facilitate the nucleation and growth of Co_3O_4 crystal.[14]

For further comparison, another kind of nitrogen-doped mesoporous graphene synthesized by a hydrothermal method was employed as the support for preparing the hybrid catalyst (denoted as Co_3O_4/MG-N).[14] Supporting Information Figure S5c shows that Co_3O_4/N-MG outperforms Co_3O_4/MG-N in terms of both half-wave potential and cathodic current, likely due to the specific chemical state of nitrogen in the doped graphene.[14,34,35] The integration of pyrrolic nitrogen atoms into graphene should contribute to the increase of electrical conductivity since they can donate two p-electrons to the π conjugated system.[24] In the case of graphitic nitrogen atoms, previous reports showed that they are more important for the ORR than the pyridinic ones.[12] Moreover, the hybridized electronic structure of pyrrolic and graphitic nitrogen atoms may also boost the adsorption of oxygen molecules on the catalyst surface and thus accelerate the ORR.[24] The significance of doping method for design and synthesis of new nitrogen-doped materials should never be underestimated.

CONCLUSIONS

In this work, a nitrogen-doped mesoporous graphene with large surface area, high porosity, and well-defined graphite framework has been developed and employed as the catalyst support for in situ loading of Co_3O_4 nanocrystals. The Co_3O_4/N-MG hybrid nanocomposite shows an excellent electrocatalytic activity for the ORR with the more positive onset overpotential as well as a higher current density through a four-electron reduction mechanism, which is comparable to Pt/C (10 wt %). The results indicate that the porous 3D structure, the conductive graphene skeleton, the existence of surface nitrogen atoms, the method of doping nitrogen into MG, and the synergistic effect between Co_3O_4 and N-MG are all crucial factors for the superior catalytic behavior of Co_3O_4/N-MG. With the tunability for different catalysts and doped elements by using various templates or precursors, this study could be very influential for preparing novel NPM catalysts in clean energy applications.

ASSOCIATED CONTENT

Supporting Information

Additional characterization and electrochemical data. This material is available free of charge via the Internet at http://pubs.acs.org.

AUTHOR INFORMATION

Corresponding Author

*Email: bhliu@fudan.edu.cn.

Notes

The authors declare no competing financial interest.

ACKNOWLEDGMENTS

This work was supported by NSFC (21375022, 21175028) and State Key Lab of Molecular Engineering of Polymers.

REFERENCES

(1) Cheng, F.; Chen, J. Metal–Air Batteries: From Oxygen Reduction Electrochemistry to Cathode Catalysts. *Chem. Soc. Rev.* **2012**, *41*, 2172–2192.

(2) Qin, Y.; Lu, J.; Du, P.; Chen, Z.; Ren, Y.; Wu, T.; Miller, J. T.; Wen, J.; Miller, D. J.; Zhang, Z.; et al. *In Situ* Fabrication of Porous-Carbon-Supported α-Mno_2 Nanorods at Room Temperature: Application for Rechargeable Li-O_2 Batteries. *Energy Environ. Sci.* **2013**, *6*, 519–531.

(3) Wang, B. Recent Development of Non-Platinum Catalysts for Oxygen Reduction Reaction. *J. Power Sources* **2005**, *152*, 1–15.

(4) Shanmugam, S.; Osaka, T. Efficient Electrocatalytic Oxygen Reduction over Metal Free-Nitrogen Doped Carbon Nanocapsules. *Chem. Commun.* **2011**, *47*, 4463–4465.

(5) Shin, S. I.; Go, A.; Kim, I. Y.; Lee, J. M.; Lee, Y.; Hwang, S.-J. A Beneficial Role of Exfoliated Layered Metal Oxide Nanosheets in Optimizing the Electrocatalytic Activity and Pore Structure of Pt-Reduced Graphene Oxide Nanocomposites. *Energy Environ. Sci.* **2013**, *6*, 608–617.

(6) Han, X.; Zhang, T.; Du, J.; Cheng, F.; Chen, J. Porous Calcium–Manganese Oxide Microspheres for Electrocatalytic Oxygen Reduction with High Activity. *Chem. Sci.* **2013**, *4*, 368–376.

(7) Nallathambi, V.; Lee, J. W.; Kumaraguru, S. P.; Wu, G.; Popov, B. N. Development of High Performance Carbon Composite Catalyst for Oxygen Reduction Reaction in PEM Proton Exchange Membrane Fuel Cells. *J. Power Sources* **2008**, *183*, 34–42.

(8) Jasinski, R. A New Fuel Cell Cathode Catalyst. *Nature* **1964**, *201*, 1212–1212.

(9) Wang, H.; Liang, Y.; Li, Y.; Dai, H. $Co_{1-x}S$-Graphene Hybrid: A High-Performance Metal Chalcogenide Electrocatalyst for Oxygen Reduction. *Angew. Chem., Int. Ed.* **2011**, *50*, 10969–10972.

(10) Kadish, K. M.; Frémond, L.; Burdet, F.; Barbe, J.-M.; Gros, C. P.; Guilard, R. Cobalt(IV) Corroles as Catalysts for the Electro-reduction of O_2: Reactions of Heterobimetallic Dyads Containing a Face-to-Face Linked Fe(III) or Mn(III) Porphyrin. *J. Inorg. Biochem.* **2006**, *100*, 858–868.

(11) Lee, D. U.; Kim, B. J.; Chen, Z. One-Pot Synthesis of a Mesoporous $NiCO_2O_4$ Nanoplatelet and Graphene Hybrid and Its Oxygen Reduction and Evolution Activities as an Efficient Bi-Functional Electrocatalyst. *J. Mater. Chem. A* **2013**, *1*, 4754–4762.

(12) Dai, L.; Chang, D. W.; Baek, J. B.; Lu, W. Carbon Nanomaterials for Advanced Energy Conversion and Storage. *Small* **2012**, *8*, 1130−1166.
(13) Liang, Y.; Wang, H.; Diao, P.; Chang, W.; Hong, G.; Li, Y.; Gong, M.; Xie, L.; Zhou, J.; Wang, J.; et al. Oxygen Reduction Electrocatalyst Based on Strongly Coupled Cobalt Oxide Nanocrystals and Carbon Nanotubes. *J. Am. Chem. Soc.* **2012**, *134*, 15849−15857.
(14) Liang, Y.; Li, Y.; Wang, H.; Zhou, J.; Wang, J.; Regier, T.; Dai, H. Co_3O_4 Nanocrystals on Graphene as a Synergistic Catalyst for Oxygen Reduction Reaction. *Nat. Mater.* **2011**, *10*, 780−786.
(15) Xu, J.; Gao, P.; Zhao, T. S. Non-Precious Co_3O_4 Nano-Rod Electrocatalyst for Oxygen Reduction Reaction in Anion-Exchange Membrane Fuel Cells. *Energy Environ. Sci.* **2012**, *5*, 5333−5339.
(16) Yu, D.; Wei, L.; Jiang, W.; Wang, H.; Sun, B.; Zhang, Q.; Goh, K.; Si, R.; Chen, Y. Nitrogen Doped Holey Graphene as an Efficient Metal-Free Multifunctional Electrochemical Catalyst for Hydrazine Oxidation and Oxygen Reduction. *Nanoscale* **2013**, *5*, 3457−3464.
(17) Liao, L.; Zhu, J.; Bian, X.; Zhu, L.; Scanlon, M. D.; Girault, H. H.; Liu, B. MoS_2 Formed on Mesoporous Graphene as a Highly Active Catalyst for Hydrogen Evolution. *Adv. Funct. Mater.* **2013**, *23*, 5326−5333.
(18) Huang, X.; Qian, K.; Yang, J.; Zhang, J.; Li, L.; Yu, C.; Zhao, D. Functional Nanoporous Graphene Foams with Controlled Pore Sizes. *Adv. Mater.* **2012**, *24*, 4419−4423.
(19) Yang, W.; Fellinger, T. P.; Antonietti, M. Efficient Metal-Free Oxygen Reduction in Alkaline Medium on High-Surface-Area Mesoporous Nitrogen-Doped Carbons Made from Ionic Liquids and Nucleobases. *J. Am. Chem. Soc.* **2011**, *133*, 206−209.
(20) Liang, J.; Jiao, Y.; Jaroniec, M.; Qiao, S. Z. Sulfur and Nitrogen Dual-Doped Mesoporous Graphene Electrocatalyst for Oxygen Reduction with Synergistically Enhanced Performance. *Angew. Chem., Int. Ed.* **2012**, *51*, 11496−11500.
(21) Zhu, J.; Tang, J.; Zhao, L.; Zhou, X.; Wang, Y.; Yu, C. Ultrasmall, Well-Dispersed, Hollow Siliceous Spheres with Enhanced Endocytosis Properties. *Small* **2010**, *6*, 276−282.
(22) Kwon, K.; Sa, Y. J.; Cheon, J. Y.; Joo, S. H. Ordered Mesoporous Carbon Nitrides with Graphitic Frameworks as Metal-Free, Highly Durable, Methanol-Tolerant Oxygen Reduction Catalysts in an Acidic Medium. *Langmuir* **2012**, *28*, 991−996.
(23) Jaouen, F.; Herranz, J.; Lefevre, M.; Dodelet, J.-P.; Kramm, U. I.; Herrmann, I.; Bogdanoff, P.; Maruyama, J.; Nagaoka, T.; Garsuch, A.; et al. Cross-Laboratory Experimental Study of Non-Noble-Metal Electrocatalysts for the Oxygen Reduction Reaction. *ACS Appl. Mater. Interfaces* **2009**, *1*, 1623−1639.
(24) Bai, J.; Zhu, Q.; Lv, Z.; Dong, H.; Yu, J.; Dong, L. Nitrogen-Doped Graphene as Catalysts and Catalyst Supports for Oxygen Reduction in Both Acidic and Alkaline Solutions. *Int. J. Hydrogen Energy* **2013**, *38*, 1413−1418.
(25) Sheng, Z. H.; Shao, L.; Chen, J. J.; Bao, W. J.; Wang, F. B.; Xia, X. Catalyst-Free Synthesis of Nitrogen-Doped Graphene via Thermal Annealing Graphite Oxide with Melamine and Its Excellent Electrocatalysis. *ACS Nano* **2011**, *5*, 4350−4358.
(26) Guo, H. L.; Wang, X. F.; Qian, Q. Y.; Wang, F. B.; Xia, X. A Green Approach to the Synthesis of Graphene Nanosheets. *ACS Nano* **2009**, *3*, 2653−2659.
(27) Nethravathi, C.; Rajamathi, M. Chemically Modified Graphene Sheets Produced by the Solvothermal Reduction of Colloidal Dispersions of Graphite Oxide. *Carbon* **2008**, *46*, 1994−1998.
(28) Davis, R. E.; Horvath, G. L.; Tobias, C. W. The Solubility and Diffusion Coefficient of Oxygen in Potassium Hydroxide Solutions. *Electrochim. Acta* **1967**, *12*, 287−297.
(29) Tammeveski, L.; Erikson, H.; Sarapuu, A.; Kozlova, J.; Ritslaid, P.; Sammelselg, V.; Tammeveski, K. Electrocatalytic Oxygen Reduction on Silver Nanoparticle/Multi-Walled Carbon Nanotube Modified Glassy Carbon Electrodes in Alkaline Solution. *Electrochem. Commun.* **2012**, *20*, 15−18.
(30) Kruusenberg, I.; Matisen, L.; Jiang, H.; Huuppola, M.; Kontturi, K.; Tammeveski, K. Electrochemical Reduction of Oxygen on Double-Walled Carbon Nanotube Modified Glassy Carbon Electrodes in Acid and Alkaline Solutions. *Electrochem. Commun.* **2010**, *12*, 920−923.
(31) Liang, Y.; Wang, H.; Zhou, J.; Li, Y.; Wang, J.; Regier, T.; Dai, H. Covalent Hybrid of Spinel Manganese−Cobalt Oxide and Graphene as Advanced Oxygen Reduction Electrocatalysts. *J. Am. Chem. Soc.* **2012**, *134*, 3517−3523.
(32) Lee, J.; Jeong, B.; Ocon, J. D. Oxygen Electrocatalysis in Chemical Energy Conversion and Storage Technologies. *Curr. Appl. Phys.* **2013**, *13*, 309−321.
(33) Yu, D.; Nagelli, E.; Du, F.; Dai, L. Metal-Free Carbon Nanomaterials Become More Active than Metal Catalysts and Last Longer. *J. Phys. Chem. Lett.* **2010**, *1*, 2165−2173.
(34) Zhang, B.; Wen, Z.; Ci, S.; Mao, S.; Chen, J.; He, Z. Synthesizing Nitrogen-Doped Activated Carbon and Probing its Active Sites for Oxygen Reduction Reaction in Microbial Fuel Cells. *ACS Appl. Mater. Interfaces* **2014**, *6*, 7464−7470.
(35) Bag, S.; Roy, K.; Gopinath, C.; Raj, C. Facile Single-Step Synthesis of Nitrogen-Doped Reduced Graphene Oxide-Mn_3O_4 Hybrid Functional Material for the Electrocatalytic Reduction of Oxygen. *ACS Appl. Mater. Interfaces* **2014**, *6*, 2692−2699.